Journal of Materials Chemistry B

ROYAL SOCIETY OF CHEMISTRY

PAPER

View Article Online
View Journal | View Issue

Cite this: J. Mater. Chem. B, 2023, 11, 10706

A metal–organic framework complex for enhancing tumor treatments through synergistic effect of chemotherapy and photodynamic therapy†

Xiang Jiang,[ab] Yuewu Zhao,*[a] Shengkai Sun,[a] Li Wang,[a] Lina Sun,[a] Wenjing Li,[a] Zheng Wang,[a] Jine Wang*[abc] and Renjun Pei*[a]

Porphyrin-based metal–organic frameworks (PMOFs) are a kind of crystal hybrid material with broad application prospects in energy, catalysis, biomedicine, and other fields. In this study, the La-TCPP PMOF nanocrystal was constructed using a porphyrin ligand and La ion. This material can produce a high loading rate on doxorubicin (DOX) owing to its special porous structure. The high loading rate of drug molecules and the reactive oxygen species (ROS) of the porphyrin ligand enable La-TCPP@DOX nanocrystal to produce a powerful killing effect on cancer cells under the synergistic attack of chemotherapy (CT) and photodynamic therapy (PDT). Finally, by modifying the targeted aptamer, the actual therapeutic effect of this special La-TCPP@DOX@Apt material on tumors was confirmed by applying the established mouse tumor model. The composite nanomaterial not only avoids the side effects caused by high concentrations of chemotherapeutic drugs, but also overcomes the limitation of PDT owing to insufficient light penetration and can inhibit and kill solid tumors under the condition of synergistic attack. This study is a complement to PMOF crystal materials, and its tumor-killing ability was achieved by loading drugs and introducing targeting molecules, which proves that the synergistic attack can more effectively inhibit and treat solid tumors. These studies have a reference and guiding significance for the treatment of cancer patients.

Received 15th July 2023,
Accepted 21st October 2023

DOI: 10.1039/d3tb01592k

rsc.li/materials-b

1. Introduction

The photodynamic therapy (PDT) is a new type of non-invasive treatment with low systemic toxicity, good spatiotemporal selectivity, high curative efficacy, and low side effects and has been widely used in practical treatments.[1] The basic principle of PDT is that the photosensitizer can be excited by energy level transition under illumination, and this activated photosensitizer further transfers the energy to molecular oxygen in tissues, producing cytotoxic reactive oxygen species (ROS), which lead to apoptosis and necrosis of cancer cells, thus achieving the purpose of effectively inhibiting tumors.[2–4] However, owing to the low penetration depth of the excitation light, such as near-infrared light, the PDT process cannot act on the deep tissue of the tumor, which seriously limits its inhibitory effect.[5] Chemotherapy (CT) as one of the main therapeutic methods used in clinics can inhibit the growth of cancer cells by local or intravenous administration, which makes it easier for therapeutic drugs to enter the deep tissues of tumors.[6] It also has many potential disadvantages, such as high concentration dependence, non-specific distribution, low cycle duration, high toxicity, and side effects.[7] If the CT and PDT are combined, it will not only reduce the concentration dependence and toxicity of chemotherapeutic drugs, but will also overcome the limitation of insufficient light penetration and can ultimately have a synergistic effect on the cancer cells of solid tumors. Therefore, it is necessary to develop new materials to achieve the synergistic effect of CT and PDT and improve the therapeutic effect on cancer patients.

Porphyrin-based metal–organic frameworks (PMOFs) are a class of crystalline material formed by the coordination of porphyrin molecules with metal ions, which has many potential applications owing to the unique structure and properties in biomedical fields, such as PDT,[8–10] biocatalyst,[11,12] biological imaging,[13,14] and drug delivery.[15–17] As a strong photosensitizer,

[a] CAS Key Laboratory of Nano-Bio Interface, Suzhou Institute of Nano-Tech and Nano-Bionics, Chinese Academy of Sciences, Suzhou, 215123, China. E-mail: ywzhao2017@sinano.ac.cn, jewang2012@sinano.ac.cn, rjpei2011@sinano.ac.cn
[b] College of Mechanics and Materials, Hohai University, Nanjing, 210098, China
[c] Jiangxi Institute of Nanotechnology, Nanchang, 330200, China

† Electronic supplementary information (ESI) available. See DOI: https://doi.org/10.1039/d3tb01592k

porphyrin can produce ROS that are toxic to cancer cells by electronic transition under light stimulation.[18,19] Therefore, the PMOF-structured materials constructed with porphyrins can not only improve the stability and biocompatibility of photosensitizers, but also enhance the PDT effect through the formation of organic ligand mono-dispersion.[20,21] Lin *et al.* developed various types of PMOF materials based on porphyrin ligands,[22–26] which not only proved that they can be effectively used in the PDT treatment of tumors but also further analyzed the influence of PMOF materials with two-dimensional and three-dimensional structures on PDT.[26] Zhou *et al.* conducted numerous studies on PMOF materials[27–29] and obtained a series of PCN-224 spherical materials with a size of 30–190 nm through precise regulation, which confirmed that 90 nm PMOF spherical particles can be preferentially ingested by cancer cells.[29] These results indicate that PMOF materials can be effectively used in the PDT treatment of tumors, but they are still influenced by multiple factors. Thus, the study and use of porphyrins to construct PMOF materials has become a feasible strategy for improving the effects of PDT.

To develop new PMOF materials, the type of adjuvant used in the synthesis process has become a problem that researchers must consider. Adjuvants can effectively increase the number of crystal nuclei and promote crystal growth,[30] which plays an important role in the synthesis of PMOF materials. In this regard, Zhang *et al.* have obtained multiple types of PMOF materials using polyvinylpyrrolidone (PVP) as an adjuvant and confirmed that polymer PVP can selectively adhere to the surface of PMOF and play a role in stabilizing and restricting the vertical growth of PMOF materials.[31–34] Based on a similar principle, our research groups have also obtained some PMOF materials using benzoic acid or biphenyldicarboxylic acid as adjuvant.[35,36] These results suggest that the adjuvant can regulate the growth of PMOF during its synthesis. Doxorubicin (DOX) is a broad-spectrum antineoplastic drug that can produce a wide range of biochemical effects on the body and has a strong cytotoxic effect. Thus, combining the antitumor characteristics of DOX with the PDT performance of PMOF may have a synergistic therapeutic effect on solid tumors. As we all know, the effective therapeutic effect of nanomedicine can be achieved only by delivering it to tumor sites. Then, the modification of nanomedicine so that it can be targeted to the tumor site has become an indispensable part. Based on these considerations, as shown in Scheme 1, the La-TCPP PMOF nanocrystal was synthesized by 4,4,4,4-(porphine-5,10,15,20-tetrayl) tetrakis (benzoic acid) (TCPP) and lanthanum chloride ($LaCl_3$) using a PVP adjuvant. PMOF nanocrystals can produce a large loading effect on small molecule drugs owing to their unique porous structure, and their exposed edges can modify small molecules with tumor targeting. This is because the exposed carboxyl groups at the edge of PMOF are easier to activate to coordinate or have a covalent reaction with the targeted molecules. Consequently, the high drug-loading capacity and photosensitive nature of PMOF enable the obtained La-TCPP@DOX@Apt to produce strong synergistic effects of CT and PDT on tumors under the modification of targeted molecules.

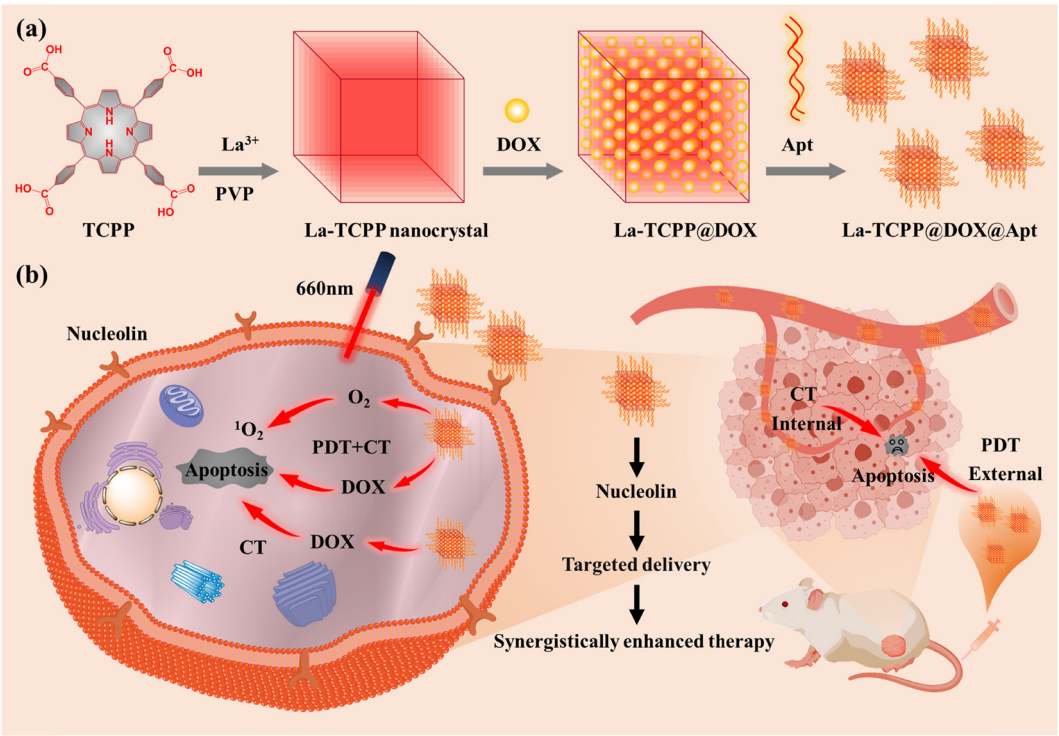

Scheme 1 Schematic illustration of the (a) preparation process and (b) synergetic enhancement of tumor therapeutic applications of La-TCPP@DOX@Apt materials.

2. Experimental section

2.1 Chemicals

4,4,4,4-(Porphine-5,10,15,20-tetrayl) tetrakis (benzoic acid) (TCPP), Lanthanum chloride hexahydrate ($LaCl_3 \cdot 6H_2O$), polyvinylpyrrolidone (PVP K30), and doxorubicin (DOX) were purchased from Aladdin Biochemical Co., Ltd. AS1411 aptamer was purchased from Shanghai Sangon Biotech. SOSG was purchased from Thermo Fisher Scientific. All other chemicals were of analytical grade and were used without further purification. Water was obtained from the Milli-Q purification system.

2.2 Synthesis of La-TCPP PMOF nanocrystals

All chemical compounds were dissolved in corresponding solvents to facilitate the subsequent addition process. Specifically, $LaCl_3 \cdot 6H_2O$ was dissolved in DMF at a concentration of 10 mM; TCPP was dissolved in DMSO at a concentration of 10 mM; and PVP K30 was dissolved in DMF at a concentration of 0.4 M (the molecular weight of PVP was calculated in the repeating unit of PVP of 111 g mol^{-1}). Then, 2.0 mL $LaCl_3 \cdot 6H_2O$, 1.0 mL TCPP, 0.5 mL PVP, and 10 mL ethanol were added into a 50 mL round bottom flask. The reaction was carried out at 120 °C for 2 h. Finally, the mixture was centrifuged at 10 000 rpm for 10 min and then washed with ethanol and water three times.

2.3 Synthesis of La-TCPP@DOX nanocrystal

Briefly, 1.0 mg La-TCPP and 2.5 mg DOX were added to 5.0 mL deionized water, and the concentrations of La-TCPP and DOX in the mixed solution were 0.2 mg mL^{-1} and 0.5 mg mL^{-1}, respectively. Then, the reaction process was carried out by stirring for 24 h at room temperature. Subsequently, the mixture was centrifuged and washed three times with water at 10 000 rpm for 10 min. A total of 15 mL of supernatant was collected after three centrifugations. According to the UV-vis spectrum of DOX in the supernatant at 480 nm, the unloaded DOX was calculated to be 1.1057 mg. Thus, the DOX loading rate was determined using the following formula: Drug content (weight%) = (weight of the feeding DOX − weight of the DOX in the supernatant)/(weight of the La-TCPP@DOX nanocrystal) × 100%. That is, (2.5 − 1.1057)/(2.5 − 1.1057 + 1.0) × 100% = 58.2%.

2.4 Synthesis of La-TCPP@DOX@Apt materials

La-TCPP@DOX (0.2 mg mL^{-1}) was incubated with 500 μL EDC aqueous solution (100 mM) and 500 μL NHS aqueous solution (100 mM) for 0.5 h at room temperature. The activated La-TCPP@DOX was mixed with 44 μL 3-NH_2-AS1411 aptamer (5′-GGTGGTGGTGGTTGTGGTGGTGGTGGAAAAAA-NH_2-3′, 140 μM) by stirring for 15 h at room temperature. The La-TCPP@DOX@Apt product was collected after being washed with water three times and stored at 4 °C.

2.5 Singlet oxygen characterization

500 μL La-TCPP PMOF nanocrystal (5 μg mL^{-1}) and 2 μL SOSG (0.5 mM) were mixed. The fluorescence spectra of the mixture were obtained at a voltage of 600 V at various intervals.

2.6 Hemocompatibility assay of La-TCPP PMOF nanocrystals

Fresh rat blood was used as a source of red blood cells. To obtain red blood cells, 2 mL fresh blood from rats was added to 10 mL PBS and centrifuged at 2000 rpm for 5 min. After washing with PBS three times, the red blood cells were diluted into 20 mL PBS disperse solution. Then, 0.4 mL erythrocytes were added to 0.8 mL La-TCPP PMOF suspension in PBS at various concentrations (2.5, 5, 10, 20, 40 and 80 μg mL^{-1}). The mixture of red blood cells and PMOF was incubated at 37 °C for 1 h and then centrifuged at 1200 rpm for 10 min. Additionally, 100 μL supernatant was taken from each sample and transferred to a 96-well plate. Finally, a microplate reader was used to measure the absorbance of the supernatant at 550 nm, and the hemolysis rate was calculated. The red blood cells treated with water and PBS were used as positive (+) and negative (−) controls, respectively. The hemolysis percentage of La-TCPP PMOF was calculated as follows: Hemolysis rate = (absorbance of sample − absorbance of negative control)/(absorbance of positive control − absorbance of negative control) ×100%.

2.7 Cell culture

The cancer cell lines (4T1 cells) were purchased from the Shanghai Chinese Academy of Sciences. The 4T1 cells were cultured in RPMI-1640 medium with 10% fetal bovine serum and 1% penicillin–streptomycin in a 5% CO_2-humidified incubator at 37 °C.

2.8 Cytotoxicity assay

The *in vitro* cytotoxicity of La-TCPP and La-TCPP@DOX was evaluated by applying the CCK-8 method. Briefly, 4T1 cells were inoculated into 96-well plates at a density of 2×10^4 cells per well and divided into two groups according to light and dark. After 24 h of culture, the early medium was replaced with a medium prepared with different concentrations of La-TCPP and La-TCPP@DOX. The dark group was further cultured for 24 hours, while the light group was treated with an additional 660 nm laser (100 mW cm^{-2}, 15 min) after 6 hours and cultured for another 20 hours.

Finally, 100 μL of FBS-free fresh medium containing 10% (v/v) CCK-8 solution was added to each hole of the 96-well plate, and the whole plate was incubated again for 1 h. The pore plate was incubated for 1 hour away from light, and the absorbance at 450 nm was read by a microplate reader (PerkinElmer Victor × 4).

2.9 Detection of intracellular ROS

The 4T1 cells were inoculated into confocal Petri dishes at a density of 1×10^5 cells per cm^2. After 24 hours, the early medium was replaced with a medium containing 20 μg mL^{-1} of La-TCPP@DOX and La-TCPP@DOX@Apt. After incubation for 6 hours, the 4T1 cells were washed three times with PBS, and an FBS-free fresh medium containing DCFH-DA ROS probes (10 mM) and Hoechst (5 mM) was added. After incubating for 30 min, the cells were exposed to a laser (200 mW cm^{-2}, 5 min). Then, the culture medium was removed, and the cells were

washed 3 times and re-suspended in PBS. Finally, an imaging analysis of ROS production capacity was performed using an Olympus FV1000-IX81 confocal laser scanning microscope (CLSM).

2.10 Cell uptake analysis

Flow cytometry analysis: The 4T1 cells were inoculated into 6-well plates according to the density of 5×10^5 cells per well. After incubation for 24 h, the early medium was replaced with a medium containing 20 μg mL^{-1} of La-TCPP@DOX and La-TCPP@DOX@Apt. One hour later, digestion treatment was performed, and the suspension was performed in a PBS buffer solution. Flow cytometry was used for detection.

CLSM analysis: The 4T1 cells were inoculated in a confocal dish at a density of 5×10^5 and incubated for 24 hours. Then, the early medium was replaced with a medium containing 20 μg mL^{-1} of La-TCPP@DOX and La-TCPP@DOX@Apt. After culturing for 3, 6 and 12 h, the contents of La-TCPP@DOX and La-TCPP@DOX@Apt in cells were observed by applying a confocal laser scanning microscope (CLSM). The location of the cells is determined by a bright field.

2.11 Live/dead cell staining

The 4T1 cells were inoculated into 48-well plates at a density of 4×10^4 cells per well. After 24 h, the early medium was replaced with a medium containing 40 μg mL^{-1} of La-TCPP, La-TCPP@DOX and La-TCPP@DOX@Apt. The control group was added the same amount of PBS. After the MOF was added to the light group for 6 h, the light group was illuminated (100 mW cm^{-2}) for 10 min. After continued incubation for 6 h, the calcium AM/PI working solution was added and incubated for 20 min. Fluorescence images were collected using a confocal laser scanning microscope (CLSM).

2.12 Cell apoptosis analysis

The 4T1 cells were inoculated into 6-well plates according to the density of 5×10^5 cells per well. After 24 h, the early medium was replaced with a medium containing 10 μg mL^{-1} of La-TCPP, La-TCPP@DOX, and La-TCPP@DOX@Apt. After 6 hours, the cells were illuminated (100 mW cm^{-2}) for 10 min. After continued culture for 18 h, the cells were isolated and collected, stained with Annexin V-FITC and PI, and analyzed by flow cytometry.

2.13 *In vivo* uptake capacity analysis

The La-TCPP@DOX and La-TCPP@DOX@Apt were intravenously injected into tumor-bearing mice at a dose of 0.5 mg kg^{-1}. The mice were sacrificed 24 hours later, and tumors and major organs were collected for *ex vivo* imaging *via* IVIS (Lumina XRMS Series) for tissue distribution study and evaluation of *in vivo* targeting ability.

2.14 Anticancer ability of materials

All animal experiments in this paper were approved by the Animal Ethics Committee of the Suzhou Institute of Nano-Tech and Nano-Bionics and were conducted in accordance with the relevant laws and institutional guidelines of the US National Institutes of Health. Female BALB/c nude mice at 4–6 weeks of age were purchased from Nanjing Skorui Biotechnology Co., Ltd.

To construct the tumor bearing nude mouse model, 4T1 cells (3×10^6 cells) were subcutaneously injected into the right side of nude mice. After 7 days, tumor-bearing mice with tumor volumes between 70 and 120 mm^3 were randomly divided into four groups (n = 5, each group). On days 0 and 4, La-TCPP, La-TCPP@DOX, and La-TCPP@DOX@Apt were administered intravenously at 0.5 mg kg^{-1} or equivalent PBS. After 24 h of injection, each group of mice was exposed to 10 min of laser (660 nm, 200 mW cm^{-2}). Mouse weight and tumor volume were recorded every two days. A vernier caliper was used to measure the length and width of the tumor (V = length × width^2/2) to determine the tumor volume (V).

The mice were sacrificed on day 14, and the removed tumors were photographed. The heart, liver, spleen, lung, and kidney of nude mice were sectioned for histological observation using hematoxylin-eosin (H&E) staining.

2.15 Characterization

The UV-vis absorption spectrum was performed using a 1280 UV-visible spectrophotometer (Shimadzu, Japan). FT-IR analysis was carried out using Nicolet Nexus 470 (Thermo, USA). The morphology and size of PMOF were investigated using field-emission scanning electron microscopy (SEM, Quanta 400 FEG, USA) and Hitachi HT7700 transmission electron microscopy (TEM), respectively. The elemental mapping images of PMOF were obtained using high-resolution TEM (HRTEM) with a Tecnai G2 F20 S-TWIN instrument. Fluorescence (FL) spectra were performed using a FluoroMax-4 spectrofluorometer with xenon discharge lamp excitation (HORIBA, USA). X-ray photoelectron spectroscopy (XPS) was obtained using a Thermo Scientific K-Alpha+ spectrometer. The Brunauer–Emmett–Teller (BET) surface area was obtained using nitrogen adsorption/desorption on an ASAP 2460 analyzer (Micromeritics, USA). A Zetasizer Nano (Malvern instrument, UK) was used to determine the hydrodynamic diameter and zeta potential. 660 nm light-emitting diodes (MW-GX-660, China) were utilized to perform the PDT and singlet oxygen experiments.

3. Results and discussion

As shown in Fig. 1(a), La-TCPP PMOF nanocrystals were obtained by the chelating reaction of TCPP and lanthanum chloride with PVP as an adjuvant. The nanomaterial has a square structure with a particle size of 100–170 nm, and its average hydrodynamic diameter is about 216.6 nm (Fig. S1, ESI†). The C, N, O, and La elements are homogeneously distributed in the elemental mapping (Fig. 1(b)), indicating that the PMOF nanocrystal is composed of TCPP and La ions. Then, the composition and microstructure of La-TCPP are further analyzed by XPS (Fig. 1(c)). The COOR peak at the binding energy (BE) 288.5 eV (Fig. S2, ESI†) confirmed the coordination reaction between the carboxyl group of porphyrin

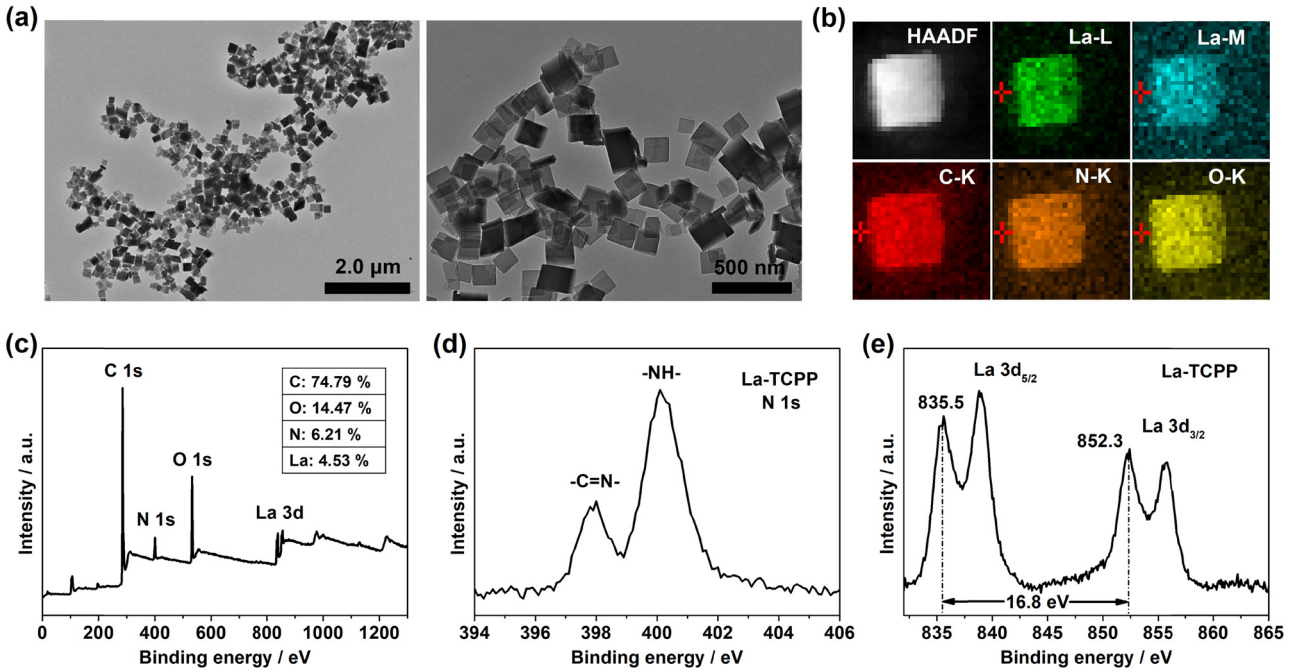

Fig. 1 (a) TEM images, (b) elemental mapping, (c) XPS spectra, (d) N 1s spectra, and (e) La 3d spectra of the prepared La-TCPP PMOF nanocrystals.

and the La ion cluster. The strong –NH– BE peak at 400.1 eV depicted in Fig. 1(d) confirms the central uncoordinated effect of TCPP porphyrin during the coordination reaction. The BE peaks of La $3d_{5/2}$ are observed at 835.5 eV and 838.8 eV, and the BE peaks of La $3d_{3/2}$ are observed at 852.3 eV and 855.6 eV, with a spin–orbital splitting interval of 16.8 eV (Fig. 1(e)). This value is consistent with the reported results,[37,38] proving that the La element is still in a +3 valence state in the PMOF structure without any change.

In addition to XPS spectra results, UV-vis, FT-IR, fluorescence, and BET analyses of La-TCPP were also performed. With the formation of La-TCPP, UV-vis absorption is slightly red-shifted and the strong Söret bands are relatively widened (Fig. 2(a)), which is caused by the formation of PMOF nanocrystals. The UV-vis absorption still showed four Q bands before and after the formation of the nanocrystals, indicating that the TCPP porphyrins did not undergo central metal coordination.[39,40] This result was further supported by the FT-IR analysis, as depicted in Fig. 2(b), where the N–H in-plane vibration at 963 cm^{-1} did not change significantly but showed only a slight displacement at 973 cm^{-1}. The C═O stretching vibration at 1683 cm^{-1} disappeared obviously, while a relatively significant infrared absorption peak appeared at 1653 cm^{-1}, indicating that coordination occurred between carboxyl groups and La ion clusters, consistent with our previous research results.[21,41] The formation of La-TCPP PMOF nanocrystals also caused changes in its band gap, leading to a slight fluorescence redshift (Fig. 2(c)). Then, the BET surface area of La-TCPP was confirmed to be 230.2 $m^2 g^{-1}$ by N_2 adsorption–desorption isotherm, and the pore size distribution showed that the PMOF nanocrystals had a micropore structure of about 1.2 nm (Fig. 2(d)). These results indicate that the nanocrystal is formed by the coordination between the carboxyl groups of TCPP porphyrin and La ion clusters, in which the La element exists in the coordination nodes of the PMOF structure in the form of a +3 valence state.

Highly biocompatibility is a prerequisite for the application of nanomaterials in the biomedical field. For this, the hemocompatibility of the synthesized La-TCPP PMOF nanocrystals was analyzed. As shown in Fig. 3(a), with the concentration increase in La-TCPP (2.5–80 μg mL^{-1}), the hemolysis rate increased from 1.43% to 21.57%. Among them, La-TCPP still exhibited a small hemolysis rate (7.22%) even at a concentration of 20 μg mL^{-1}, which proves that the PMOF nanocrystals have excellent hemocompatibility. Subsequently, the cytotoxicity of La-TCPP was investigated to further determine its biocompatibility. The results showed that La-TCPP had low cytotoxicity, and the PMOF nanocrystals did not show obvious toxicity even at the concentration of 100 μg mL^{-1} (Fig. S3, ESI†). However, photo-stimulated La-TCPP showed a strong killing effect on cancer cells, and the survival rate of cancer cells decreased to 18.9% at a concentration of 20 μg mL^{-1} (Fig. 3(d)). This is because porphyrin organic ligands can maximize the production of singlet oxygen ($^1O_2$) with cytotoxicity in the PMOF structure[42–44] and can show an obvious PDT effect in a relatively short time (Fig. S4, ESI†). Based on the excellent hemocompatibility and low toxicity characteristics of La-TCPP PMOF nanocrystals, they can be effectively applied in fields related to tumor therapy.

La-TCPP PMOF nanocrystals have a large specific surface area and may also show outstanding effects in loading anticancer drugs. Here, we demonstrated that doxorubicin (DOX) can be efficiently loaded into PMOF structures through

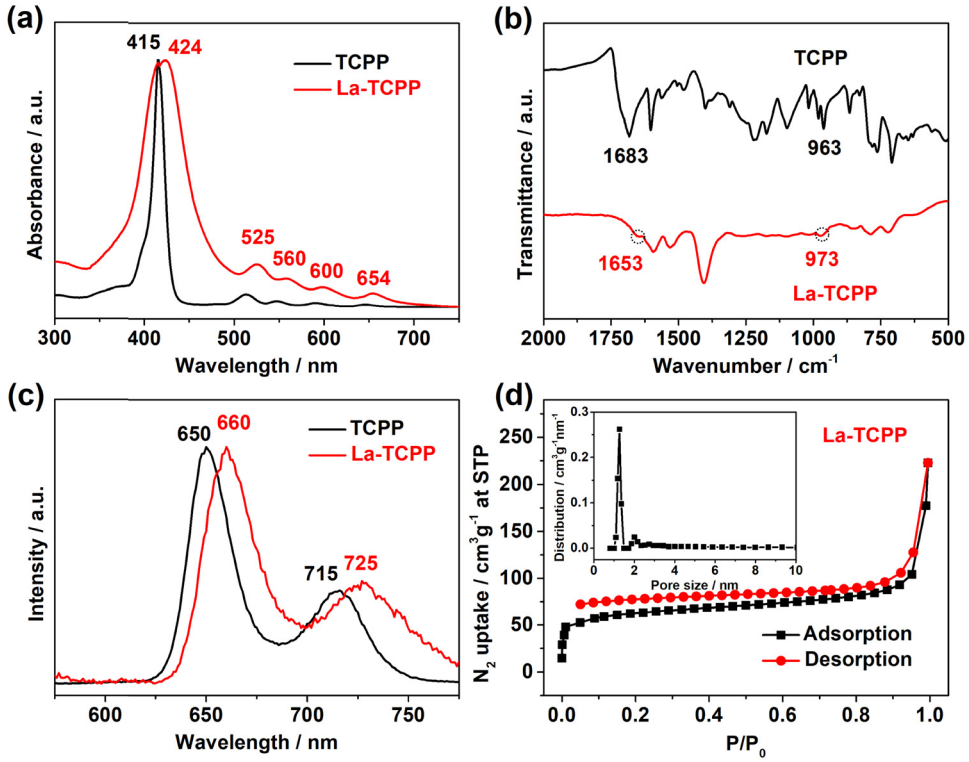

Fig. 2 (a) UV-vis absorption, (b) FT-IR, and (c) fluorescence spectra of TCPP and La-TCPP. (d) N_2 adsorption–desorption isotherms and the corresponding pore size distribution curve of the prepared La-TCPP PMOF nanocrystals.

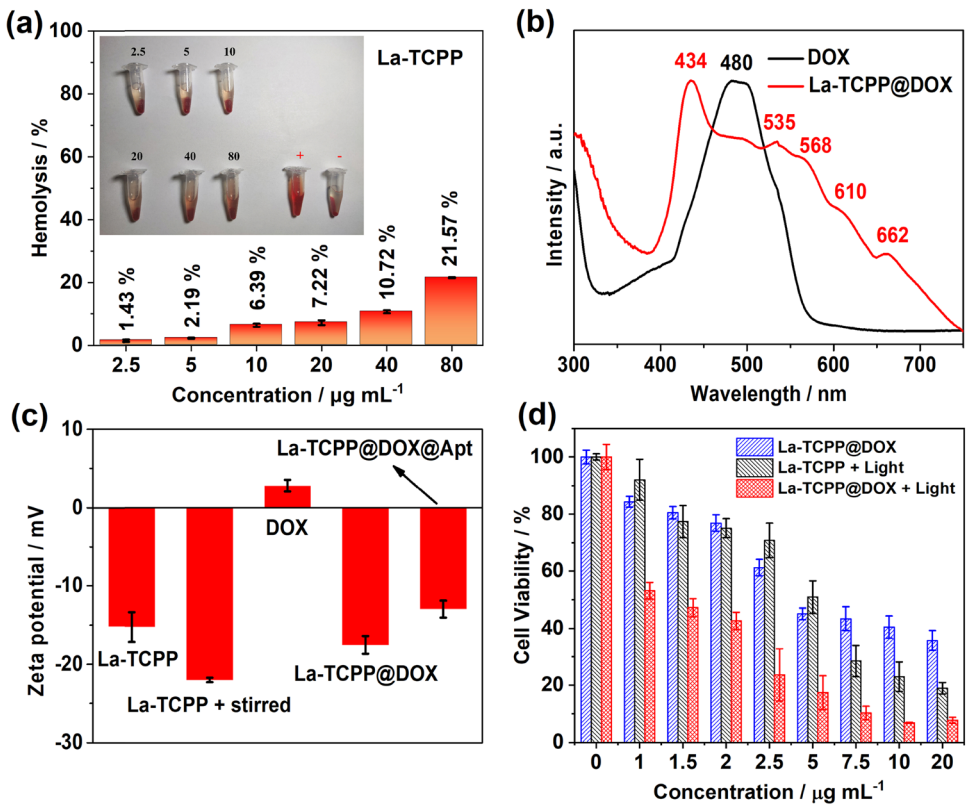

Fig. 3 (a) Effect of different concentrations of La-TCPP on the hemolysis rate of red blood cells after 1 h of incubation. (b) UV-vis absorption of DOX and La-TCPP@DOX. (c) Zeta potential of La-TCPP, La-TCPP + stirred, DOX, La-TCPP@DOX, and La-TCPP@DOX@Apt. (d) Relative viability of 4T1 cells treated with La-TCPP@DOX, La-TCPP + light, and La-TCPP@DOX + light. Laser conditions: 660 nm, 100 mW cm^{-2}, and 15 min.

electrostatic interactions. As shown in Fig. 3(b), the La-TCPP@DOX showed the characteristic UV-vis absorption peaks of PMOF nanocrystals and displayed a broad absorption range around 480 nm, indicating the successful loading of DOX. Notably, the loading of DOX made the original UV-vis absorption peak of La-TCPP red-shift by about 10 nm (Fig. 2(a) and 3(b)), which may be caused by the increase in hydrodynamic diameter after loading (Fig. S5, ESI†). The loading efficiency of DOX onto the PMOF nanocrystals was determined by measuring the UV-vis absorption of the residual fluid after loading (Fig. S6, ESI†), and there is a linear relationship between the UV-vis absorption and the concentration curves of DOX (Fig. S7, ESI†). It is calculated that the loading efficiency of DOX on La-TCPP@DOX nanocrystal is about 58.2% (weight%). The La-TCPP@DOX obtained by electrostatic adsorption showed relatively high stability, and its morphology and particle size (Fig. S8, ESI†) did not change significantly after one week of PBS immersion (pH = 7.4). Then, the zeta potential was used to characterize the results of loading DOX onto La-TCPP PMOF nanocrystals. Surprisingly, after adding DOX with a positive potential of about 2.8 mV, the potential of La-TCPP@DOX changed from −15.2 mV of PMOF to −17.5 mV (Fig. 3(c), La-TCPP and La-TCPP@DOX), which is a puzzling result. Considering the stirring process that always exists during the loading process, the influence of the stirring process was analyzed. Mechanical stirring causes partial disruption of the La-TCPP nanocrystals, leading to the exposure of more carboxyl groups (Fig. S9, ESI†), resulting in a lower potential of about −22 mV for the PMOF materials (Fig. 3(c), La-TCPP + stirred). This destructive effect on the PMOF structure is also reflected in the DLS results, which show a smaller hydrodynamic diameter of 215.5 nm (Fig. S10, ESI†). Therefore, during the preparation of La-TCPP@DOX, its zeta potential is influenced by two factors. First, mechanical agitation can cause partial disruption of PMOF nanocrystals, leading to a decrease in zeta potential. Second, there is an electrostatic interaction between DOX and La-TCPP, which can increase zeta potential. Under the combination of two effects, the zeta potential of La-TCPP@DOX

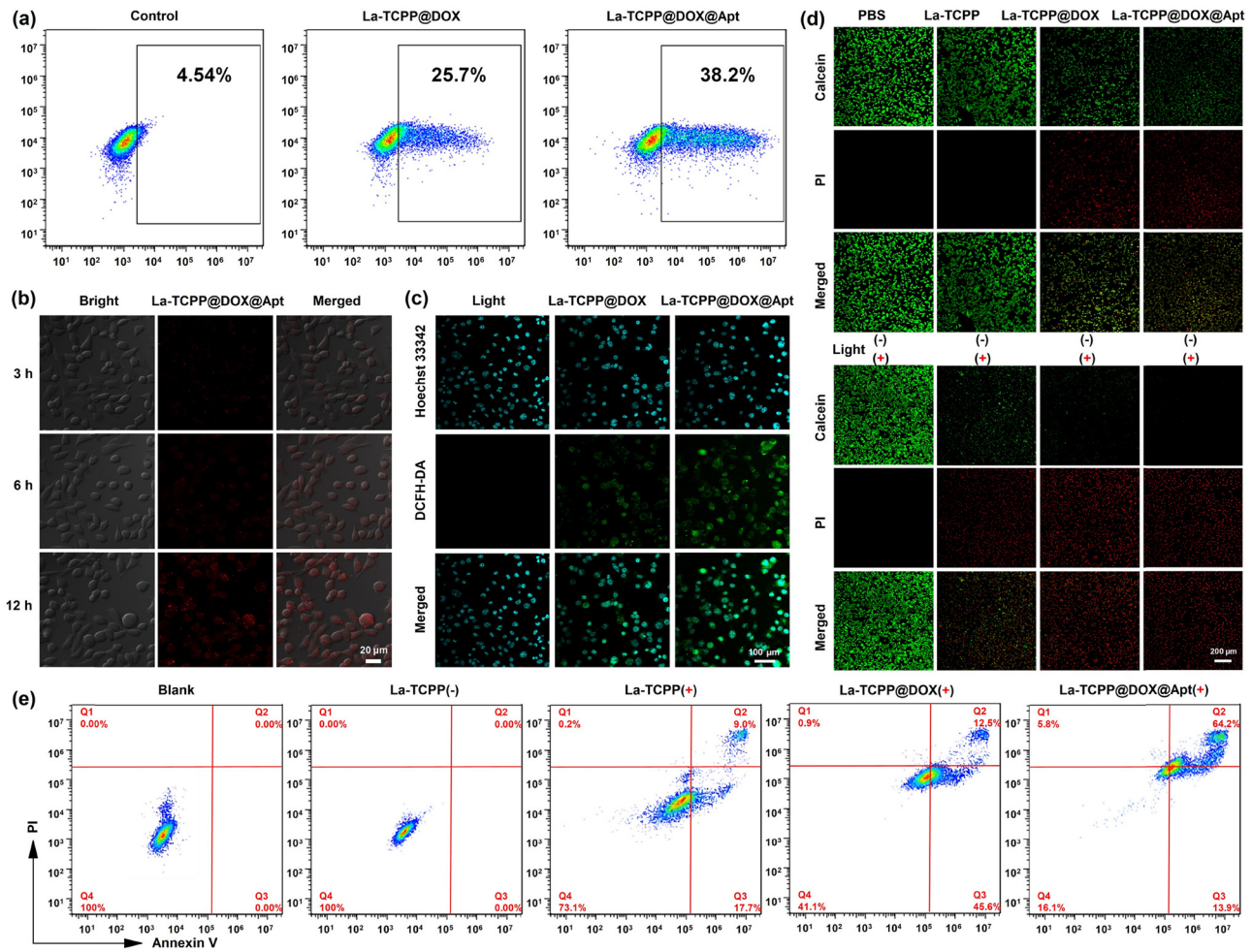

Fig. 4 (a) Analysis of the targeting ability of La-TCPP@DOX@Apt *via* flow cytometry. (b) Cellular uptake of La-TCPP@DOX@Apt in 4T1 cell incubation at different times. (c) DCFH-DA staining images of 4T1 cells after treatments with blank, La-TCPP@DOX, and La-TCPP@DOX@Apt. (d) Fluorescence images of calcein/PI co-stained 4T1 cells incubated with PBS, La-TCPP, La-TCPP@DOX, and La-TCPP@DOX@Apt in dark and light conditions. (e) Analysis of changes in apoptosis and necrosis of 4T1 cells by flow cytometry.

is measured to be −17.5 mV. Later, the cytotoxicity of DOX-loaded La-TCPP@DOX was analyzed. As shown in Fig. 3(d), at the same concentration of 20 μg mL^{-1}, La-TCPP@DOX decreased the survival rate of cancer cells to about 7% with the synergistic effect of drug therapy and photodynamic therapy. As expected, La-TCPP@DOX also responded to chemotherapy against cancer cells under non-light conditions but with a relatively high cell survival rate of about 35.7%, which is due to the chemotherapy effect of DOX drugs (Fig. S11, ESI†). These results indicate that La-TCPP nanocrystals loaded with DOX can further improve the therapeutic effect on tumor cells based on the synergistic effects of chemotherapy and photodynamic therapy.

More efficient delivery of PMOF nanomaterials to tumor sites is essential for tumor treatment. Thus, DNA aptamer AS1411 was covalently linked with the co-incubation method, and the zeta potential of La-TCPP@DOX@Apt was increased to −12.9 mV (Fig. 3(c)). DNA aptamers can specifically target cancer cells that overexpress nucleolin so that La-TCPP@DOX@Apt loaded with anticancer drugs can be delivered to tumor sites more effectively, thus generating stronger therapeutic effects on tumors. As shown in Fig. 4(a), the La-TCPP@DOX@Apt with targeting aptamer modified could target 4T1 cancer cells more effectively, from 25.7% to 38.2% simultaneously. The cancer cells could further phagocytize La-TCPP@DOX@Apt with the extension of time, and the red fluorescence of the materials could be clearly observed in the cancer cells at 12 hours (Fig. 4(b)). In addition, the uptake capacity of La-TCPP@DOX@Apt by 4T1 cancer cells was significantly greater than that of mouse fibroblast cells (L929 normal cells, Fig. S12, ESI†), which verified the special targeting ability of La-TCPP@DOX@Apt to cancer cells. After that, the intracellular ROS production capacity of La-TCPP@DOX and La-TCPP@DOX@Apt was monitored using 2′,7′-dichlorodihydrofluorescein diacetate (DCFH-DA) as ROS probes.[45,46] As shown in Fig. 4(c), the 4T1 cells without materials did not exhibit green fluorescence, while the 4T1 cells treated with La-TCPP@DOX and La-TCPP@DOX@Apt both detected strong green fluorescence. Furthermore, Apt targeting modified La-TCPP@DOX@Apt has stronger green fluorescence; this is because the targeted La-TCPP@DOX@Apt can bind with the nucleolin protein on the surface of 4T1 cells[47,48] and then pour more into cancer cells. The targeting effect of Apt was also verified in a calcein/PI (green/red, live/dead) co-staining assay of cancer cells. As shown in Fig. 4(d), neither PBS nor La-TCPP caused significant apoptosis of 4T1 cells in the absence of light, while La-TCPP@DOX and

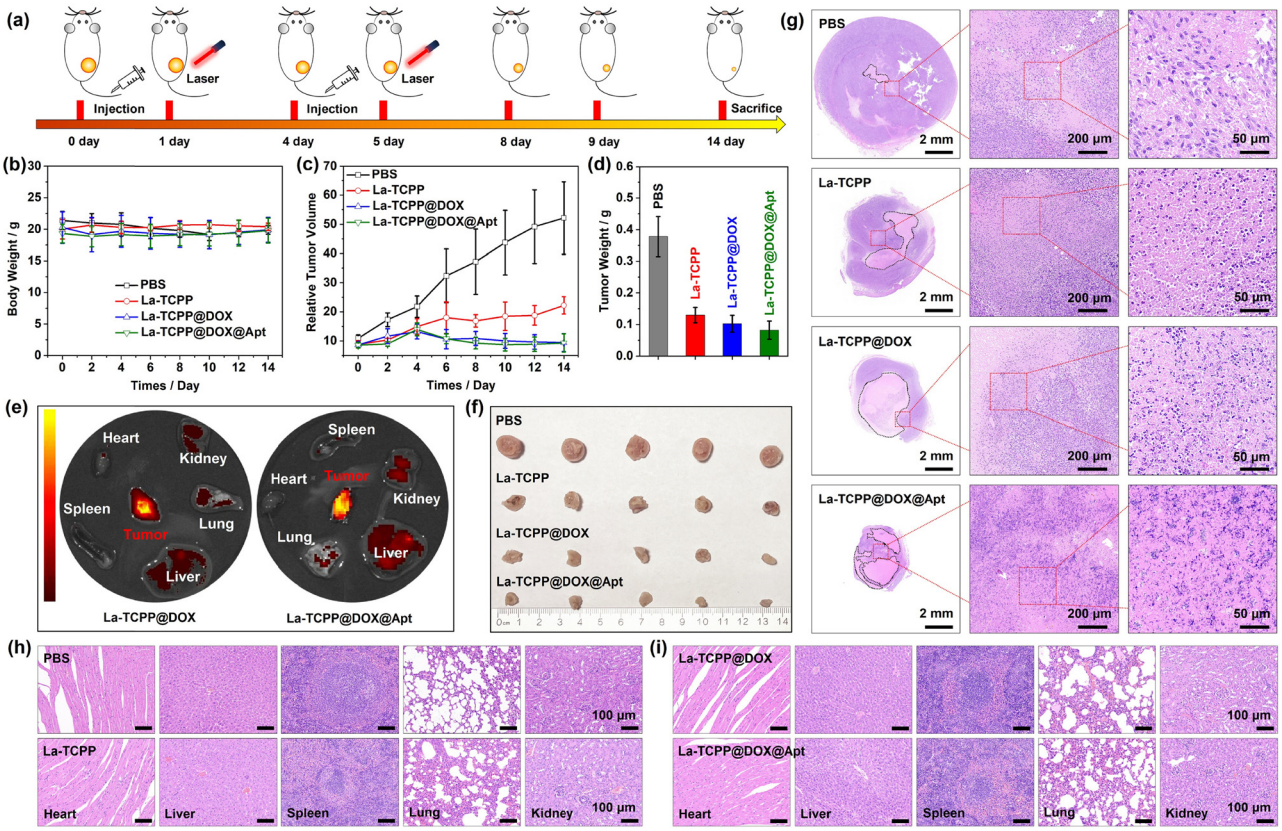

Fig. 5 (a) Schematic diagram of the treatment of tumor-bearing mice. (b) Body weight, (c) relative tumor volume, and (d) tumor weight of tumor-bearing mice after treatment with PBS, La-TCPP, La-TCPP@DOX, and La-TCPP@DOX@Apt. (e) Fluorescence images of major organs obtained 24 hours after La-TCPP@DOX and La-TCPP@DOX@Apt were intravenously injected into the tail of tumor-bearing mice. Tumor (f) photographs and (g) H&E-stained images of tumor-bearing mice obtained after 14 days of treatment with PBS, La-TCPP, La-TCPP@DOX, and La-TCPP@DOX@Apt. (h), (i) H&E-stained images of the major organs harvested from PBS, La-TCPP, La-TCPP@DOX, and La-TCPP@DOX@Apt groups.

La-TCPP@DOX@Apt both showed certain toxicity to 4T1 cells, which is mainly owing to the chemotherapy effects of DOX. Based on the targeting effect of Apt, La-TCPP@DOX@Apt resulted in relatively more dead cells. Upon exposure to light, La-TCPP, La-TCPP@DOX, and La-TCPP@DOX@Apt can produce a large number of ROS, which has a strong killing effect on cancer cells. Among them, La-TCPP@DOX and La-TCPP@DOX@Apt showed better killing effects on 4T1 cells under the synergistic action of chemotherapy and PDT. Subsequently, the related apoptosis of 4T1 cells treated with La-TCPP, La-TCPP@DOX, and La-TCPP@DOX@Apt was analyzed by flow cytometry. As shown in Fig. 4(e), compared with blank and La-TCPP(−) samples, the La-TCPP, La-TCPP@DOX, and La-TCPP@DOX@Apt showed early and late apoptosis after light exposure, and the proportion of late apoptosis based on a targeted modification of La-TCPP@DOX@Apt reached 64.2%. These results suggest that DOX incorporation into the PMOF structure can synergistically enhance the killing effect on 4T1 cancer cells and that this killing effect can be further enhanced by modifying the targeted molecules.

To further analyze the actual therapeutic effect of La-TCPP@DOX@Apt on tumors, a 4T1 tumor model of mice was designed. As shown in Fig. 5, PBS, La-TCPP, La-TCPP@DOX, and La-TCPP@DOX@Apt were used as therapeutic agents for tumor treatment in tumor-bearing mice for 14 days. In the course of treatment, the laser irradiation time was about one day later than the intravenous injection time because La-TCPP@DOX and La-TCPP@DOX@Apt could effectively gather at the tumor site after 24 hours (Fig. 5(e)). Similar results were also obtained by detecting the biological distribution of La elements in mice using inductively coupled plasma mass spectrometry (ICP-MS, Fig. S13, ESI†). Moreover, La-TCPP@DOX@Apt showed a higher concentration of aggregation at tumor sites under the targeting effect of aptamers, displaying a relatively brighter fluorescence. The weight of the mice did not fluctuate significantly throughout the treatment period (Fig. 5(b)), while the relative volume and weight of the tumors differed significantly depending on the treatment agents. As shown in Fig. 5(c), compared with the PBS treatment group, La-TCPP inhibited the growth of the tumor under the action of ROS, but the tumor still increased slowly owing to the penetration depth of the laser. After DOX drugs were added, DOX could be released in the slightly acidic environment of tumors (Fig. S14, ESI†), which made the La-TCPP@DOX and La-TCPP@DOX@Apt experimental groups successfully inhibit the growth of tumors under the synergistic effect of chemotherapy and PDT. The higher material aggregation induced by targeting makes La-TCPP@DOX@Apt exhibit a higher tumor therapeutic effect (Fig. 5(d)). After that, the mice were sacrificed, and the obtained solid tumors were compared and analyzed. As shown in Fig. 5(f) and (g), the tumor-bearing mice treated with PBS, La-TCPP, La-TCPP@DOX, and La-TCPP@DOX@Apt showed an obvious decreasing trend in tumor size. Moreover, the hematoxylin & eosin (H&E) stained results of the tumor section confirmed that 4T1 cancer cells in the PBS group were active and dense, and there was only a small blank area in the tumor center. In the groups treated with La-TCPP, La-TCPP@DOX, and La-TCPP@DOX@Apt, the blank area in the tumor center was obviously enlarged, and the adjacent 4T1 cells showed early and late apoptotic states. As shown in the enlarged Fig. 5(g), the 4T1 cells in PBS, La-TCPP, La-TCPP@DOX, and La-TCPP@DOX@Apt groups showed oval, round, semi-ruptured, and completely ruptured morphologies, respectively, which further indicated that these 4T1 cells were in normal, early and late apoptotic stages.

Finally, the major organs of the treated tumor-bearing mice were H&E stained and analyzed. As shown in Fig. 5(h) and (i), compared with the PBS group, no changes were observed in the heart, liver, spleen, lung, and kidney of La-TCPP, La-TCPP@DOX, and La-TCPP@DOX@Apt groups, indicating that these materials did not cause significant histological damage to major tissues and had lower biological toxicity. These results confirmed that La-TCPP@DOX@Apt has a low toxicity and high biocompatibility, which can effectively target tumor tissue within 24 hours and have a strong killing effect on tumor cells under the synergistic effect of chemotherapy and photodynamic therapy, thus achieving the goal of successfully inhibiting tumors. Therefore, the La-TCPP PMOF nanocrystals can effectively load anticancer drugs, and La-TCPP@DOX@Apt can be used as an effective chemotherapy and photodynamic therapy agent for tumors under the action of targeted aptamers.

4. Conclusions

In summary, La-TCPP PMOF nanocrystals were successfully constructed using the bottom-up method. The porous structure of the La-TCPP PMOF nanocrystal can produce a strong loading capacity, and the loading rate of DOX reached 58.2%. This high drug loading rate and ROS capability enable La-TCPP@DOX to produce a strong therapeutic effect on tumors under the synergistic attack of chemotherapy and PDT. Moreover, the tumor targeting performance of La-TCPP@DOX@Apt was achieved by introducing the targeting aptamer, demonstrating its high killing effect on 4T1 tumor cells at both cellular and animal levels. This study confirmed that the porous structure of PMOF can effectively carry small molecule drugs and can be used as an effective nanomedicine to inhibit tumors by introducing the targeted aptamer. These findings provide valuable guidance and a foundation for the preparation of PMOF materials and the development of tumor therapy.

Author contributions

Xiang Jiang: data collection in cells and animals. Yuewu Zhao: conceptualization, methodology, formal analysis, investigation, writing–original draft, writing–review & editing, funding acquisition, and supervision. Shengkai Sun: synthesis of PMOF materials. Li Wang, Lina Sun, Wenjing Li, and Zheng Wang: technical guidance and assistance in the experiments. Jine Wang and Renjun Pei: writing–review & editing, funding acquisition, and supervision.

Conflicts of interest

The authors declare no competing financial interest.

Acknowledgements

This work was supported by the National Natural Science Foundation of China (32071392), the Natural Science Foundation of Jiangsu Province (BE2023732, BE2020766, BK20221264), the China Postdoctoral Science Foundation (2021T140500), the Jiangsu Planned Projects for Postdoctoral Research Funds (2021K070A), the Science Foundation of Jiangxi Province (20192ACB21033), the Basic Research Pilot Project in Suzhou (SJC2022006), Gusu Innovation and Entrepreneurship Leading Talents Program (ZXT2022007), and the Special Cultivation Project of SINANO, CAS.

References

1 W. Fan, P. Huang and X. Chen, *Chem. Soc. Rev.*, 2016, **45**, 6488.
2 M. C. DeRosa and R. J. Crutchley, *Coord. Chem. Rev.*, 2002, **233**, 351.
3 J. Zhao, W. Wu, J. Sun and S. Guo, *Chem. Soc. Rev.*, 2013, **42**, 5323.
4 R. A. Cairns, I. S. Harris and T. W. Mak, *Nat. Rev. Cancer*, 2011, **11**, 85.
5 Z. Xiao, Q. Chen, Y. Yang, S. Tu, B. Wang, Y. Qiu, Y. Jiang, Q. Huang and K. Ai, *Chem. Eng. J.*, 2022, **449**, 137889.
6 B. A. Chabner and T. G. Roberts, *Nat. Rev. Cancer*, 2005, **5**, 65.
7 W. Fan, B. Yung, P. Huang and X. Chen, *Chem. Rev.*, 2017, **117**, 13566.
8 J. Chen, Y. Zhu and S. Kaskel, *Angew. Chem., Int. Ed.*, 2021, **60**, 5010.
9 K. Lu, C. He and W. Lin, *J. Am. Chem. Soc.*, 2015, **137**, 7600.
10 M. Lismont, L. Dreesen and S. Wuttke, *Adv. Funct. Mater.*, 2017, **27**, 1606314.
11 F. Du, L. Liu, Z. Wu, Z. Zhao, W. Geng, B. Zhu, T. Ma, X. Xiang, L. Ma, C. Cheng and L. Qiu, *Adv. Mater.*, 2021, **33**, 2101095.
12 J. Mu, L. He, W. Fan, W. Tang, Z. Wang, C. Jiang, D. Zhang, Y. Liu, H. Deng, J. Zou, O. Jacobson, J. Qu, P. Huang and X. Chen, *Small*, 2020, **16**, 2004016.
13 Z. Wang, Q. Sun, B. Liu, Y. Kuang, A. Gulzar, F. He, S. Gai, P. Yang and J. Lin, *Coord. Chem. Rev.*, 2021, **439**, 213945.
14 W. Zhu, Y. Yang, Q. Jin, Y. Chao, L. Tian, J. Liu, Z. Dong and Z. Liu, *Nano Res.*, 2019, **12**, 1307.
15 Y. Ding, H. Xu, C. Xu, Z. Tong, S. Zhang, Y. Bai, Y. Chen, Q. Xu, L. Zhou, H. Ding, Z. Sun, S. Yan, Z. Mao and W. Wang, *Adv. Sci.*, 2020, **7**, 2001060.
16 Y. Wang, J. Yan, N. Wen, H. Xiong, S. Cai, Q. He, Y. Hu, D. Peng, Z. Liu and Y. Liu, *Biomaterials*, 2020, **230**, 119619.
17 K. Kim, S. Lee, E. Jin, L. Palanikumar, J. H. Lee, J. C. Kim, J. S. Nam, B. Jana, T. H. Kwon, S. K. Kwak, W. Choe and J. H. Ryu, *ACS Appl. Mater. Interfaces*, 2019, **11**, 27512.
18 J. Zhu, C. Chu, D. Li, X. Pang, H. Zheng, J. Wang, Y. Shi, Y. Zhang, Y. Cheng, E. Ren, J. Cheng, X. Chen and G. Liu, *Adv. Funct. Mater.*, 2019, **29**, 1904056.
19 D. Wang, L. Niu, Z. Y. Qiao, D. B. Cheng, J. Wang, Y. Zhong, F. Bai, H. Wang and H. Fan, *ACS Nano*, 2018, **12**, 3796.
20 K. Lu, C. He and W. Lin, *J. Am. Chem. Soc.*, 2014, **136**, 16712.
21 Y. Zhao, Y. Kuang, M. Liu, J. Wang and R. Pei, *Chem. Mater.*, 2018, **30**, 7511.
22 K. Lu, C. He, N. Guo, C. Chan, K. Ni, R. R. Weichselbaum and W. Lin, *J. Am. Chem. Soc.*, 2016, **138**, 12502.
23 K. Ni, T. Aung, S. Li, N. Fatuzzo, X. Liang and W. Lin, *Chem*, 2019, **5**, 1892.
24 K. Lu, C. He, N. Guo, C. Chan, K. Ni, G. Lan, H. Tang, C. Pelizzari, Y. X. Fu, M. T. Spiotto, R. R. Weichselbaum and W. Lin, *Nat. Biomed. Eng.*, 2018, **2**, 600.
25 G. Lan, K. Ni, S. S. Veroneau, X. Feng, G. T. Nash, T. Luo, Z. Xu and W. Lin, *J. Am. Chem. Soc.*, 2019, **141**, 4204.
26 T. Luo, Y. Fan, J. Mao, E. Yuan, E. You, Z. Xu and W. Lin, *J. Am. Chem. Soc.*, 2022, **144**, 5241.
27 D. Feng, Z. Y. Gu, J. R. Li, H. L. Jiang, Z. Wei and H. C. Zhou, *Angew. Chem., Int. Ed.*, 2012, **51**, 10307.
28 J. Park, M. Xu, F. Li and H. C. Zhou, *J. Am. Chem. Soc.*, 2018, **140**, 5493.
29 J. Park, Q. Jiang, D. Feng, L. Mao and H. C. Zhou, *J. Am. Chem. Soc.*, 2016, **138**, 3518.
30 S. Xu, D. Cao, Y. Liu and Y. Wang, *Cryst. Growth Des.*, 2022, **22**, 2001.
31 M. Zhao, Y. Wang, Q. Ma, Y. Huang, X. Zhang, J. Ping, Z. Zhang, Q. Lu, Y. Yu, H. Xu, Y. Zhao and H. Zhang, *Adv. Mater.*, 2015, **27**, 7372.
32 Y. Wang, M. Zhao, J. Ping, B. Chen, X. Cao, Y. Huang, C. Tan, Q. Ma, S. Wu, Y. Yu, Q. Lu, J. Chen, W. Zhao, Y. Ying and H. Zhang, *Adv. Mater.*, 2016, **28**, 4149.
33 Q. Lu, M. Zhao, J. Chen, B. Chen, C. Tan, X. Zhang, Y. Huang, J. Yang, F. Cao, Y. Yu, J. Ping, Z. Zhang, X. J. Wu and H. Zhang, *Small*, 2016, **12**, 4669.
34 M. Zhao, Q. Lu, Q. Ma and H. Zhang, *Small Methods*, 2017, **1**, 1600030.
35 Y. Zhao, L. Jiang, L. Shangguan, L. Mi, A. Liu and S. Liu, *J. Mater. Chem. A*, 2018, **6**, 2828.
36 Y. Zhao, J. Wang and R. Pei, *J. Am. Chem. Soc.*, 2020, **142**, 10331.
37 G. Yan, Y. Wang, Z. Zhang, Y. Dong, J. Wang, C. Carlos, P. Zhang, Z. Cao, Y. Mao and X. Wang, *Nano-Micro Lett.*, 2020, **12**, 49.
38 K. Zou, T. Zhou, Y. Chen, X. Xiong, W. Jing, X. Dai, M. Shi, N. Li, J. Sun, S. Zhang, C. Zhang, Y. Liu and Z. Guo, *Adv. Energy Mater.*, 2022, **12**, 2103981.
39 A. A. Sinelshchikova, S. E. Nefedov, Y. Y. Enakieva, Y. G. Gorbunova, A. Y. Tsivadze, K. M. Kadish, P. Cheng, A. Bessmertnykh-Lemeune, C. Stern and R. Guilard, *Inorg. Chem.*, 2013, **52**, 999.
40 B. W. Xu, R. J. Niu, Q. Liu, J. Y. Yang, W. H. Zhang and D. J. Young, *Dalton Trans.*, 2020, **49**, 12622.
41 Y. Zhao, J. Wang, X. Cai, P. Ding, H. Lv and R. Pei, *ACS Appl. Mater. Interfaces*, 2020, **12**, 23697.
42 W. Yu, W. Zhen, Q. Zhang, Y. Li, H. Luo, J. He and Y. Liu, *ChemMedChem*, 2020, **15**, 1766.

43 Z. W. Jiang, Y. C. Zou, T. T. Zhao, S. J. Zhen, Y. F. Li and C. Z. Huang, *Angew. Chem., Int. Ed.*, 2020, **132**, 3326.
44 J. Tian, B. Huang, M. H. Nawaz and W. Zhang, *Coord. Chem. Rev.*, 2020, **420**, 213410.
45 L. Wang, X. Qu, Y. Zhao, Y. Weng, G. I. N. Waterhouse, H. Yan, S. Guan and S. Zhou, *ACS Appl. Mater. Interfaces*, 2019, **11**, 35228.
46 Z. H. Zhu, Y. Liu, C. Song, Y. Hu, G. Feng and B. Z. Tang, *ACS Nano*, 2022, **16**, 1346.
47 R. Yazdian-Robati, P. Bayat, F. Oroojalian, M. Zargari, M. Ramezani, S. M. Taghdisi and K. Abnous, *Int. J. Biol. Macromol.*, 2020, **155**, 1420.
48 W. Wang, Y. Wang, M. Ma, H. J. Jin and X. Li, *ACS Appl. Mater. Interfaces*, 2022, **14**, 44029.